JOURNAL OF SOLID STATE CHEMISTRY 34, 199–205 (1980)

Ion Exchange Properties of β-Eucryptite ($LiAlSiO_4$): EPR Investigation on Copper-Doped Single Crystals

JEAN-LOUIS BERCHOT, DANIEL VIVIEN, DIDIER GOURIER, JEANINE THERY, AND ROBERT COLLONGUES

Laboratoire de Chimie Appliquée de l'Etat Solide, L.A. 302, ENSCP 11, rue P. et M. Curie, 75231, Paris Cedex 05, France

Received January 24, 1979, in revised form August 21, 1979

Investigation of the ion exchange properties of β-eucryptite ($LiAlSiO_4$) single crystals indicates that it is impossible to substitute Li^+ by other bigger univalent cations such as Na^+, K^+, or Ag^+. On the contrary, Li^+ exchange by bivalent cations, Cu^{2+} or Mn^{2+}, is very easy. For a general orientation of the crystal with respect to the magnetic field, the EPR spectrum of Cu^{2+} ions in β-eucryptite consists of 12 sharp lines partially superimposed on a broad line. The sharp lines are attributed to isolated copper ions in the conducting channels. Cu^{2+} lies in sixfold coordinated Li″ sites, but not in the fourfold coordinated Li′ sites. The corresponding spin Hamiltonian parameters at $T = 140$ K are found to be: $g_x = 2.362$, $g_y = 2.340$, $g_z = 1.990$; $|A_x| = 85 \times 10^{-4}$ cm^{-1}, $|A_y| = 71 \times 10^{-4}$ cm^{-1}, $|A_z| = 203 \times 10^{-4}$ cm^{-1}. The broad line is attributed to clusters of Cu^{2+} located in neighboring Li″ sites.

1. Introduction

Superionic conductors are of current interest in this laboratory. The most famous of these materials is probably β-alumina, a sodium aluminate in which conductivity arises from the migration of Na^+ along the mirror planes of the structure (*1*). It has been shown that the conductivity of this material can be modified by insertion of foreign ions at low concentration either during the synthesis, or after ionic exchange of the pure compound in molten salts. The localization, which strongly depends on the doping method, of some of these ions (Mn^{2+}, Cu^{2+}) has been determined using EPR (*2–4*).

Furthermore, a doping paramagnetic ion, like Cu^{2+} ion serves as a probe to study the mobility of the conducting cations and the crystalline disorder which prevails around this ion (*5*).

The lithium aluminosilicate, $LiAlSiO_4$, β-eucryptite, also exhibits a high ionic conductivity and can be used as a solid electrolyte in high-energy density battery systems.

Li^+ ion can easily migrate in the channels of the structure parallel to the c axis of the hexagonal cell and this accounts for the high ionic monodimensional conductivity (*6*).

$$E \| c: \sigma = 1.8 \times 10^{-1} (\Omega \text{ cm})^{-1}$$

$$E \perp c: \sigma = 2 \times 10^{-4} (\Omega \text{ cm})^{-1} \text{ at } 600°C$$

In the light of our previous results on β-alumina, we have been led to undertake a similar EPR study on β-eucryptite.

2. Structure

The β-eucryptite, $LiAlSiO_4$, has an hexagonal structure (space group $P6_422$) (*7, 8*) which is a derivative of the β-quartz structure. Starting from the framework of

0022-4596/80/110199-07$02.00/0

β-quartz, half of the Si^{4+} ions are replaced by Al^{3+} ions, and the charge is balanced by introduction of Li^+ in the main channels of the structure, parallel to the 6_4 axis (i.e., c axis). Layers of Si and Al ions separated by layers of oxygen are stacked in an ordered and alternated way along the c axis.

At room temperature, the lithium ions occupy half of the available Li′ sites which are surrounded by four oxygens. It is possible then to distinguish two sorts of channels parallel to the c axis of the structure: one central channel, where Li^+ ions occupy sites within layers of Al ions, and three equivalent secondary channels, where Li^+ ions occupy sites within layers of silicium (*9*).

The vanishing of some spots at $T > 460$°C on the X-ray diffraction pattern and the thermal expansion data have been interpreted (*9*) in terms of a statistical distribution of Li^+ ions in all the fourfold coordinated sites (Li′) of the channels. This reversible dynamical Li disorder process is possible only if the Li^+ pass through a sixfold coordinated site (Li″) (Fig. 1) when they jump from an occupied Li′ site to an unoccupied site. A more detailed description of the Li″ site will be given in Sect. 5.1.

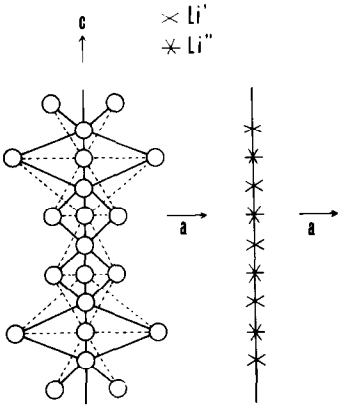

FIG. 1. Li′ (fourfold coordinated) sites and Li″ (sixfold coordinated) sites in the main channels of the structure of β-eucryptite. The interatomic bonds between the lithium sites and the coordinating oxygen atoms apart from the c axis, are represented by solid and broken lines, respectively.

3. Synthesis of β-Eucryptite and Ionic Exchange Properties

Powder samples of β-eucryptite have been synthesized by solid state reaction (at 1100°C) using stoichiometric amounts of SiO_2, Al_2O_3, and Li_2CO_3. Single crystals have been grown by the flux method described by Tscherry and Laves (*10*). A mixture containing 46.4% eucryptite, 10.3% AlF_3, 23.2% LiF, and 14.1% V_2O_5 by weight is heated in a platinum crucible at 1200°C. After homogenization of the melt, the temperature is lowered to 1130°C and the mixture is slowly cooled (1°C/hr) down to 1000°C and then, at a faster rate, to room temperature. Laue X-ray diffraction patterns and rotating crystal photographs taken with Cu$K\alpha$ X-ray radiation indicate that they are good single crystals and confirm their belonging to the $P6_422$ space group.

In order to study the ion exchange properties, some crystals about 2–3 mm diameter and 1–1.5 mm high were dipped for more than 2 days in several molten salts.

$AgNo_3$ at 500 K

$NaNO_3$ at 590 K

KNO_3 at 620 K

It was impossible to detect any weight change or modifications in positions and intensity of the diffraction lines on the Debye–Scherrer pattern of the treated crystals. This indicates that Na^+, K^+, and Ag^+ ions are unable to substitute Li^+ by ionic exchange. Because of the size of the channels these ions are probably too large to enter the structure and the size of Li^+ ion ($r = 0.60$ Å) appears to be a maximum for univalent cations.

However, crystals dipped for a few minutes in molten Cu_2Cl_2–2 wt% $CuCl_2$ at 700 K, in $CuCl_2$ at 900 K, or in molten $MnCl_2$ at 950 K have, respectively, brown or

pink color and exhibit EPR spectra characteristic of Cu^{2+} or Mn^{2+} ions in the lattice (*11*). For longer periods of treatment the crystals become brittle and are eventually completely destroyed. No attempt was made to characterize these highly exchanged products because we were mainly interested in the EPR study by low doping rates.

On the contrary, several doping experiments, in molten $LiCl–CuCl_2$ with different LiCl concentrations and various temperatures were completely unsuccessful. Among the reasons which account for the easy replacement of Li^+ by Cu^{2+} or Mn^{2+}, it can be noticed that the ionic radii of Cu^{2+} ($r = 0.69$ Å) and Mn^{2+} ($r = 0.80$ Å) are very close to that of Li^+. The electrical charge of the ions is probably also an important factor.

The ESR spectra of Cu^{2+} or Mn^{2+} disappear by dipping the copper- or manganese-doped crystals in molten $LiNO_3$ at 550 K. This indicates that the Li^+ exchange is reversible, a property which seems consistent with our unsuccessful doping experiments in $LiCl–CuCl_2$.

Further ESR studies have been limited to Cu^{2+} because it gives much simpler ESR spectra ($I = \frac{3}{2}$; $S = \frac{1}{2}$) than Mn^{2+} ($I = \frac{5}{2}$; $S = \frac{5}{2}$). However, Mn^{2+}, which has the same charge and an ionic radius similar to that of Cu^{2+}, is expected to occupy the same kind of sites.

It has been found that the mixture $Cu_2Cl_2–CuCl_2$ (2 wt%) was better than pure $CuCl_2$ for the doping process. Because of the large ionic radius of Cu^+ (equivalent to that of Na^+) this ion cannot substitute Li^+ in the structure and the low melting point compound Cu_2Cl_2 only acts as a solvent for $CuCl_2$ allowing a lower doping rate.

The EPR spectra were obtained on an X-band spectrometer fitted with a variable temperature device. The microwave radiation frequency was measured with an accuracy of 1 MHz by means of a tunable resonant cavity and the magnetic field was calibrated with a proton NMR probe.

4. Experimental Results

The spectra were recorded at room temperature, 140 K, and 3.6 K.

For a general orientation of the magnetic field with respect to the crystal axes, the spectrum consists of 12 sharp lines partially superimposed on a broad line.

4.1. Analysis of the Sharp-Line Spectrum

When the magnetic field is parallel to the c axis of the structure, the 12 lines collapse into four which arise from hyperfine interaction between the Cu^{2+} unpaired electron and the ^{65}Cu, ^{63}Cu nucleus ($I = \frac{3}{2}$). The lines are generally too broad ($\Delta H = 15–50$ G at 140 K) to allow resolution of hyperfine components of the two isotopes (ratio of the g_N factors = 1.072). This separation only appears for some orientations on the high-field ($|M_I| = 3/2$) components.

For a rotation of the magnetic field in the (a^*, b) plane, the spectrum shows a 60° periodicity in agreement with the hexagonal symmetry of the structure, and it consists of three sets of four hyperfine lines, two of the three sets being equivalent along the a^* and b direction (Fig. 2). The g value which corresponds to the center of the high-field set of lines of the a^* direction, is very close to 2. The Cu^{2+} ion principal components of the g tensor are generally bigger than or similar to the free electron value (*12*) as a result of the negative sign of the spin–orbit coupling constant. One could then infer that a^* is one of the principal axes of the g tensor. Angular variation in the (a^*, c) and (b, c) plane confirms this assumption and shows that b and c are the two other principal axes of the g tensor. The spacing of the hyperfine lines presents extremum values along these three axes, so they are also principal axes of the hyperfine A tensor.

The anisotropy of the linewidth is important at room temperature and is still present at 3.6 K although the lines are sharper at this temperature.

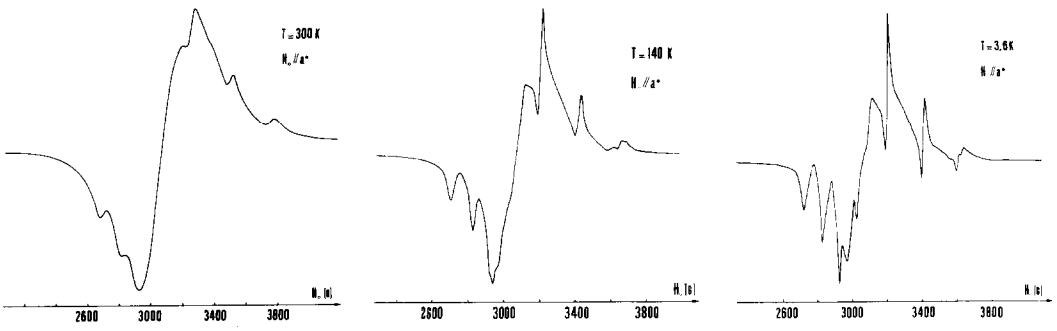

FIG. 2. EPR spectra of β-eucryptite for $H_0 \| a^*$ at 300, 140, and 3.6 K. Two of the three sets of four hyperfine lines are superimposed along this direction (because they are equivalent).

The principal values of the g and A tensors corresponding to the following spin Hamiltonian,

$$\hat{H} = \sum_{i=x,y,z} (g_i \beta \hat{H}_i \hat{S}_i + A_i \hat{S}_i \hat{I}_i),$$

have been determined at $T = 140$ K, a temperature which allows a good resolution of the spectra. The results are given in Table I.

The g and A values along the b and c axes are quite similar. Consequently, the x and y axes of the tensors are chosen along b and c, respectively, and the z axis along a^*.

4.2. *Analysis of the Broad-Line Spectrum*

Whatever the doping conditions, the intense broad line is always present in the spectra, but vanishes when the crystal is reexchanged in molten $LiNO_3$.

Its intensity accounts for 80–95% of the total spectrum and decreases when the doping time is reduced.

For a given sample, the relative intensity of the broad line is reduced by a factor of 2, when the temperature at which the spectra are recorded is lowered from 140 to 3.6 K.

The linewidth is orientation dependent, being 110 G along c, 270 G along b, and 360 G for $H_0 \| a^*$ at room temperature. The band becomes narrower at low temperature but is never resolved into several hyperfine components.

To the accuracy allowed by the important linewidth, the line appears isotropic when the field rotates in the (a^*, b) plane and its position can be described by an axially symmetric g tensor, the principal components of which are:

$$g\| = 2.42, \quad c \text{ axis},$$
$$g\perp = 2.13, \quad (a^*, b) \text{ plane}.$$

TABLE I

A AND g PRINCIPAL VALUES FOR $T = 140$ K

A_x (cm^{-1})	A_y (cm^{-1})	A_z (cm^{-1})	g_x	g_y	g_z
85×10^{-4}	71×10^{-4}	203×10^{-4}	2.362	2.340	1.990

5. Discussion

The sharp and broad ESR lines are both attributed to Cu^{2+} ions located in the channels, instead of the framework of the structure because of the following arguments:

(i) the doping conditions (short time and low temperature) are probably too mild to allow diffusion of Cu^{2+} into the Al and Si sites;

(ii) these Cu^{2+} ions are easily reexchanged by Li^+;

(iii) the localization of Cu^{2+} in the channels is in agreement with the observed periodicity of the ESR spectra.

5.1. *Localization of the "Sharp-Line Spectrum' Cu^{2+} Ion*

These lines arise from isolated Cu^{2+} ion. It has been already pointed out (Sect. 2) that two sites (Li', Li") can be occupied by cations in the channels.

The spectrum which is detected at room temperature does not come from Cu^{2+} localized in tetrahedral Li' sites, because the spin-lattice relaxation time of Cu^{2+} ion in such coordination at 300 K is very short (*13*) and this prevents observation of the ESR spectrum unless the temperature has been sufficiently lowered (a few degrees Kelvin) to increase the T_1 value.

The 3.6 K spectrum does not contain new lines with respect to the room temperature spectrum, so there is no Cu^{2+} in Li' sites and the 12-line spectrum is attributed to Cu^{2+} in six-fold coordinated Li" sites.

For Cu^{2+} in sixfold coordination, with rhombic distortion, neglecting the contribution of 4*s*, 4*p*, and ligand orbitals, the ground-state wave function may be written:

$$\Psi = \alpha|x^2-y^2> + \xi|3z^2-r^2>.$$

In first approximation, the L_z operator has no matrix elements between $|3z^2-r^2\rangle$ and any other *d* wave functions so, any difference $\Delta g_z > 0$ between g_z and the free electron *g* value will result from the contribution of $|x^2-y^2\rangle$.

In our case, g_z is very close to 2.0; this indicates that $\alpha \simeq 0$ and $\xi \simeq 1$. The very small negative Δg_z value (−0.01 at 140 K) arises from the second-order term $(-3\lambda^2/\Delta E^2_{xz})$ in the g_z expression (*14*), and also perhaps from a small 4*p* orbital mixing into the ground state. Starting from an octahedral cordination, a $|3z^2-r^2\rangle$ ground state for Cu^{2+} will result from a tetragonal contraction along the $z(a^*)$ axis. That is exactly what is observed for the Li" site depicted in Fig. 3. For this site with point symmetry C_2, the two shortest cation–oxygen distances are along the a^* axis (Table III).

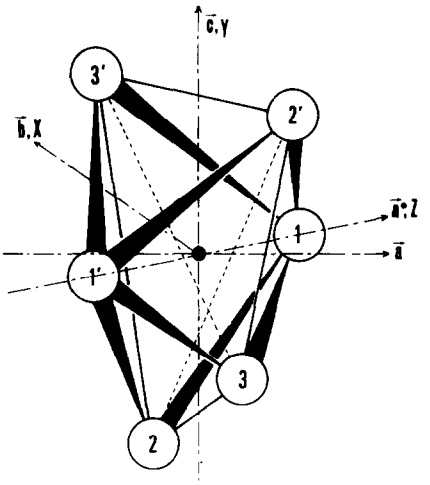

FIG. 3. Li" site: the lithium at the origin of the *a*, *b*, and *c* axes is surrounded by the six oxygen atoms, O_1, O'_1, O_2, O'_2, O_3, and O'_3. The *X*, *Y*, and *Z* axes of the *A* and *g* tensors are also indicated. The interatomic distances O_i–O'_i ($i = 1, 2, 3$) are given in Table III.

In molecular orbital approximation, the principal components of the hyperfine tensor can be calculated using the following expressions (*14, 15*) neglecting the ligand orbital contributions:

$$\frac{A_x}{p} = -K(\alpha^2+\xi^2) + \frac{2}{7}(\alpha^2-\xi^2) - \frac{4(3^{1/2})}{7}\alpha\xi + \Delta g_x - \frac{1}{14}\left(\frac{3\alpha+3^{1/2}\xi}{\alpha-3^{1/2}\xi}\right)\Delta g_y + \frac{3^{1/2}}{14}\frac{\xi}{\alpha}\Delta g_z$$

TABLE II

K, α, AND ξ VALUES OBTAINED FROM THE FOUR DIFFERENT SIGN COMBINATIONS OF A_x AND A_y HYPERFINE PARAMETERS

	1[a]	2	3	4
A_x (cm^{-1})	0.0085	0.0085	−0.0085	−0.0085
A_y (cm^{-1})	0.0071	−0.0071	0.0071	−0.0071
K	−0.102	0.030	0.056	0.187
α	0.74	1.13	1.29	1.44
ξ	0.03	−0.20	0.21	−0.03

[a] Case number.

TABLE III
INTERATOMIC DISTANCES AND ANGLES

Li′–Li′	1.86 Å	$\widehat{O_1Li''O_1} = 180°$
Li′–Li″	0.93 Å	$\widehat{O_2Li''O_2'} = 140°$
Li″–O_1, Li″–O_1'	1.82 Å	$\widehat{O_3Li''O_3'} = 140°$
Li″–O_2, Li″–O_2', Li″–O_3, Li–O_3'	2.65 Å	
O_2–O_2', O_3–O_3'	5.00 Å	
O_1–O_1'	3.64 Å	

$$\frac{A_y}{p} = -K(\alpha^2+\xi^2)+\frac{2}{7}(\alpha^2-\xi^2)+\frac{4(3^{1/2})}{7}\alpha\xi - \frac{1}{14}\left(\frac{3\alpha-3^{1/2}\xi}{\alpha+3^{1/2}\xi}\right)\Delta g_x + \Delta g_y - \frac{3^{1/2}}{14}\frac{\xi}{\alpha}\Delta g_z,$$

$$\frac{A_z}{p} = -K(\alpha^2+\xi^2)-\frac{4}{7}(\alpha^2-\xi^2) + \frac{1}{14}\left(\frac{3\alpha-3^{1/2}\xi}{\alpha+3^{1/2}\xi}\right)\Delta g_x + \frac{1}{14}\left(\frac{3\alpha+3^{1/2}\xi}{\alpha-3^{1/2}\xi}\right)\Delta g_y + \Delta g_z$$

which give

$$(A_x+A_y+A_z)/p+3K = \Delta g_x+\Delta g_y+\Delta g_z.$$

In these expressions p is the free ion dipolar parameter (360×10^{-4} cm^{-1} for Cu^{2+}), and K the isotropic Fermi contact term. The absolute signs of the A parameters are unknown, but because of the predominantly $|3z^2-r^2\rangle$ ground state, one can infer that A_z is positive.

Taking each of the four possibilities for the signs of A_x and A_y and using the preceding equations, one can deduce the four sets of K, α, and ξ values which are gathered in Table II. Replacing A_x and Δg_x by A_y and Δg_y introduces only a change in the sign of α, so that the labeling of x and y axes does not affect the absolute values of K, α, and ξ. Δg_x and Δg_y, on the one hand, and A_x and A_y, on the other hand, are very similar. This suggests that A_x and A_y have the same sign (cases 1 and 4, Table II). Furthermore for the last three sets of A_x and A_y values, one gets $\alpha > 1$. The only combination which gives reasonable values of α and ξ is $A_x = +0.0085$ cm^{-1}; $A_y = +0.0071$ cm^{-1}. It implies a negative value for the Fermi contact term: $K = -0.102$. Generally, K is positive, of the order of 0.2 to 0.4 (*16*).

This unusual negative sign can be understood by considering that the K value results from various contributions (*16*):

– exchange polarization of the unpaired electron with filled inner 1*s* and 2*s* copper orbitals. This produces a negative spin density at the nucleus and gives a positive contribution to K.

—3*s* shell contribution which can be positive or negative depending upon the relative distribution of the 3*s* and 3*d* orbitals.

In our case, the Cu^{2+} site is compressed along the g tensor z axis. This could have affected the radial distribution of the electron in the $3z^2-r^2$ orbital, causing the 3*s* orbital to be outside of the $3z^2-r^2$ one. Therefore, the contribution of the 3*s* shell polarization could be negative.

—direct contribution of the 4*s* orbital unpaired electron density, the sign of which is negative. For Cu^{2+} in C_2 symmetry, this contribution occurs through mixing of $|3z^2-r^2\rangle$ and $|4s\rangle$ which belongs to the same irreducible representation.

It is then possible that the negative contributions predominate in our case, accounting for the resultant negative sign for K.

5.2. Localization of the "Broad-Line Spectrum" Cu^{2+} Ion

In contrast with the sharp-line spectrum attributed to isolated Cu^{2+} ions in Li″ sites, the broad line could arise from interacting Cu^{2+} ions located in neighboring Li″ sites.

Pairs or clusters of Cu^{2+} ions lined up in the same channel should have their g_z tensor axis parallel to the pair or cluster axis (e.g.,

the channel axis as it has been found experimentally on our crystals (see Sect. 4.2)).

The electron spin for a pair of Cu^{2+} ions (*17*), in which the isotropic exchange interaction is stronger than the anisotropic contributions, will be equal to 1, as for copper acetate, giving a triplet-state ESR spectrum.

In our case one observes only a single line indicating that we are dealing with clusters of Cu^{2+} ions rather than with pairs.

Taking into account that the $x(b)$ and $z(a^*)$ axes of two neighboring Li″ sites are rotated $2\pi/3$ apart, the g tensor components of the clusters in the (a^*, b) plane, should result from a certain averaging of g_x and g_z for Cu^{2+} ion in an isolated Li″ site (*17*). This is actually observed because the 143 K g value (2.12) of the clusters is intermediate between 2.36 and 1.99.

The distance between two Li″ sites is short ($d = 1.86$ Å) but the magnetic interaction between two neighboring Cu^{2+} ions would probably occur through the oxygen ions surrounding the Li″ site rather than by a direct overlapping of Cu^{2+} orbitals, which should give a metal–metal bond.

This superexchange mechanism should give an antiferromagnetic coupling between Cu^{2+} ions which is consistent with a decrease in the intensity of the broad line by lowering the temperature. Knowing that the formation of Cu^{2+} clusters is very easy, one can suggest that some kind of cooperative mechanism, which leads to clustering of the Cu^{2+} ions, operates during the doping process.

One can think, for instance, that a Cu^{2+} ion in the Li″ site distorts the lattice in such a way that neighboring Li″ sites become more accessible to other Cu^{2+} ions.

References

1. R. COLLONGUES, J. THERY, AND J. P. BOILOT, *in* "Solid Electrolytes" (P. Hagenmuller and W. Van Gool, Eds.), p. 253, Academic Press, New York (1978).
2. J. P. BOILOT, A. KAHN, J. THERY, R. COLLONGUES, J. ANTOINE, D. VIVIEN, C. CHEVRETTE, AND D. GOURIER, *Electrochim. Acta* **22**, 741 (1977).
3. D. GOURIER, J. ANTOINE, D. VIVIEN, J. THERY, J. LIVAGE, AND R. COLLONGUES, *Phys. Status Solidi A* **41**, 423 (1977).
4. D. GOURIER, D. VIVIEN, J. THERY, J. LIVAGE, AND R. COLLONGUES, *Phys. Status Solidi A* **45**, 599 (1978).
5. A. ROCKENBAUER AND P. SIMON, *J. Magn. Reson.* **18**, 320 (1975).
6. U. V. ALPEN, M. SCHULZ, AND G. M. TALAT, *Solid State Commun.* **23**, 911 (1977).
7. V. TSCHERRY, M. SCHULZ, AND F. LAVES, *Z. Kristallogr.* **135**, 161 (1972).
8. V. TSCHERRY, M. SCHULZ, AND F. LAVES, *Z. Kristallogr.* **135**, 175 (1972).
9. M. SCHULZ, *J. Amer. Ceram. Soc.* **57**, 313 (1974).
10. V. TSCHERRY AND F. LAVES, *Naturwissenschaften* **57**(4), 194 (1970).
11. A. ABRAGAM AND B. BLEANEY, "Résonance Paramagnetique des ions de transitions," Presses Univ. France, Paris (1971).
12. J. E. WERTZ AND J. R. BOLTON, "Electron Spin Resonance," McGraw–Hill, New York (1972).
13. J. W. ORTON, "Electron Paramagnetic Resonance," Iliffe, London (1968).
14. B. BLEANEY, K. D. BOWERS, AND M. H. L. PRYCE, *Proc. Roy. Soc. London Ser. A* **228**, 166 (1955).
15. E. BULUGGIU, G. DASCOLA, D. C. GIORI, AND A. VERA, *J. Chem. Phys.* **54**, 2191 (1971).
16. J. R. PILBROW AND J. M. SPAETH, *Phys. Status Solidi* **20**, 237 (1967).
17. J. OWEN AND E. A. HARRIS, *in* "Electron Paramagnetic Resonance" (S. Geschwind, Ed.), p. 427, Plenum, New York, (1972).